



Trans. Nonferrous Met. Soc. China 35(2025) 3493–3506

Transactions of Nonferrous Metals Society of China

www.tnmsc.cn



# Efficient recovery of metallic aluminum from hazardous secondary aluminum dross via ball-milling and supergravity-enhanced separation

Zeng-wu WANG, Jin-tao GAO, Xi LAN, Zhan-cheng GUO

State Key Laboratory of Advanced Metallurgy, University of Science and Technology Beijing, Beijing 100083, China

Received 23 January 2024; accepted 3 July 2024

**Abstract:** Secondary aluminum dross (SAD), a by-product of aluminum extraction from primary aluminum dross, contains metallic aluminum particles coated with dense oxidized films, complicating the recovery of metallic aluminum using traditional methods. Ball-milling was employed to break and alter the structure of these oxidized films. The results indicated that the films became thinner and stripped away, exposing the aluminum surface. Based on the in-situ observation of the structure evolution of milled SAD particles with temperature, the metallic aluminum liquid was efficiently recovered from SAD at 680 °C via supergravity-enhanced separation, where the recovery ratio and mass fraction of Al in the separated aluminum phase were up to 95.72% and 99.10 wt.%, respectively. Moreover, the tailings can be harmlessly utilized in refractory, cement and ceramic fields with subsequent treatment, such as denitrification, dechlorination, and fluoride fixation.

Key words: secondary aluminum dross (SAD); metallic aluminum; efficient recovery; ball-milling; supergravity-enhanced separation

#### 1 Introduction

Metallic aluminum is mainly produced from bauxite ore through Bayer digestion, Hall-Héroult electrolysis, and subsequent smelting process [1–3]. During the smelting of electrolytic aluminum, a substantial portion of aluminum liquid undergoes oxidation, resulting in the formation of primary aluminum dross (PAD), which coats the surface of the aluminum liquids [4]. The hot PAD is removed from the smelting furnace and includes a mass of aluminum droplets [5]. Generally, about 40 kg of PAD is generated per ton of molten aluminum [6], and the growing global demand for aluminum metal has led to significant losses of aluminum in PAD.

In recent decades, the physical agitation method has been increasingly applied to extracting

metallic aluminum from the hot PAD with higher efficiency and lower cost, for the sake of linking up the production process of aluminum. The discharged hot PAD undergoes mechanical agitation in an iron pan along with some flux, allowing the aluminum liquid to flow at the bottom of the agitator under the influence of gravity, after which it is collected and utilized [7]. However, due to the vigorous agitation, the aluminum liquid comes into full contact with air and undergoes heavy oxidation, leading to the encapsulation of some unrecovered fine aluminum droplets by dense solid films, which then flow into the hot residual dross [8]. Typically, the hot residual dross is cooled, crushed, and transformed into another byproduct known as secondary aluminum dross (SAD) [9].

SAD has been regarded as hazardous solid waste according to the Catalogue of Hazardous

Wastes in Europe since 2002 [10] and the National Waste List of China in 2021 [11]. In a humid environment, the SAD in contact with water vapor or rainwater will release lots of flammable and perilous gases such as methane, phosphine, hydrogen disulfide, and ammonia [12], leading to severe air pollution [13]. Additionally, the disposal of SAD in landfills can cause salts to permeate through water and soil, posing a threat to the stability of the ecological environment [14]. Moreover, the dust pollution generated by fine SAD particles can be detrimental to human health [15]. Therefore, the extensive accumulation of SAD not only results in a significant loss of aluminum but also contributes to environmental pollutants [16]. Many countries have implemented stringent environmental protection laws that prohibit the open-air stacking or landfilling of SAD due to its leachability, irritant properties, toxicity, and reactivity [17].

disposal safe and comprehensive utilization of SAD pose a global challenge. Recently, SAD utilization has focused on preparing building materials [18], ceramic materials [19], and refractory materials [20,21]. Resource recovery from SAD primarily involves extracting Al<sub>2</sub>O<sub>3</sub> using acid [22,23], alkali routes [24,25], or other methods [26,27]. However, the yield of metallic aluminum in current treatments remains extremely low due to the fine size and severe oxidation of SAD [25,28]. Therefore, there is a need to develop a more effective method to disrupt the oxidized films coating the metal particles and enhance the separation of aluminum liquid from SAD. Generally, ball-milling is widely employed to augment the surface area of metallic aluminum particles by activating and changing the structure of oxidized films [29,30]. Moreover, the supergravity method has been reported to be significant for enhancing solid-liquid or liquid-liquid separation in complex systems at high temperatures [31,32], so it can be introduced to enhance the separation and recovery of metallic aluminum resources from SAD.

In this study, a novel approach that combines ball-milling and supergravity-enhanced separation is proposed to efficiently recover metallic aluminum from SAD. The surface structure of SAD particles before and after ball-milling is investigated, in-situ observations of the surface structure evolution of SAD particles with

temperature are conducted, and the supergravityenhanced separation of metallic aluminum liquid from SAD is examined. Furthermore, both the metallic aluminum product and the tailings are characterized and discussed, providing insights into the efficient recovery of metallic aluminum and the sustainable utilization of SAD.

### 2 Experimental

### 2.1 Characterization and analytical methods

The scanning electron microscope device equipped with the energy-dispersive X-ray spectrum (SEM-EDS, MLA250, FEI Quanta) and X-ray diffractometer (XRD, Smartlab, Rigaku) were used to analyze the microstructure and phase composition of raw material and experimental samples. The chemical composition of the original particles and mass fraction of aluminum in different parts of experimental samples were measured by an inductively coupled plasma—atomic emission spectrometer (ICP-AES, Plasma1000, NCS Testing Technology Co., Ltd.) and chemical analysis.

### 2.2 Material

The hot PAD, generated during the refining process of electrolytic aluminum at the Shanxi Al-smelter in China, was converted into SAD after extracting a proportion of aluminum through agitation, as illustrated in Fig. 1. The SAD, which still contained a substantial amount of fine aluminum droplets, was adopted as the raw material for this study. The initial SAD material was granular, charcoal gray in color, and consisted of uneven agglomerates with a maximum size of roughly 5 mm, along with many tiny particles. The SAD was first sieved using a set of sieves (ISO 565) with specified sizes to get its grain size distribution. Each 1.3 kg sample was taken from the upper, middle, and bottom portions of the barrel containing freshly created SAD, then sieved through 18 mesh and 50 mesh standard sieves, dried, and weighed for each sample.

According to the actual weighted results, the particles with sizes >1.00 mm, 0.300-1.00 mm, and <0.300 mm were named D1, D2, and D3 particles, respectively, and their macroscopic morphologies are shown in Fig. 2(a). The mass of D1, D2, and D3 particles accounted for 45.54%, 39.39%, and 15.07% of the whole SAD, as listed in Table 1. In

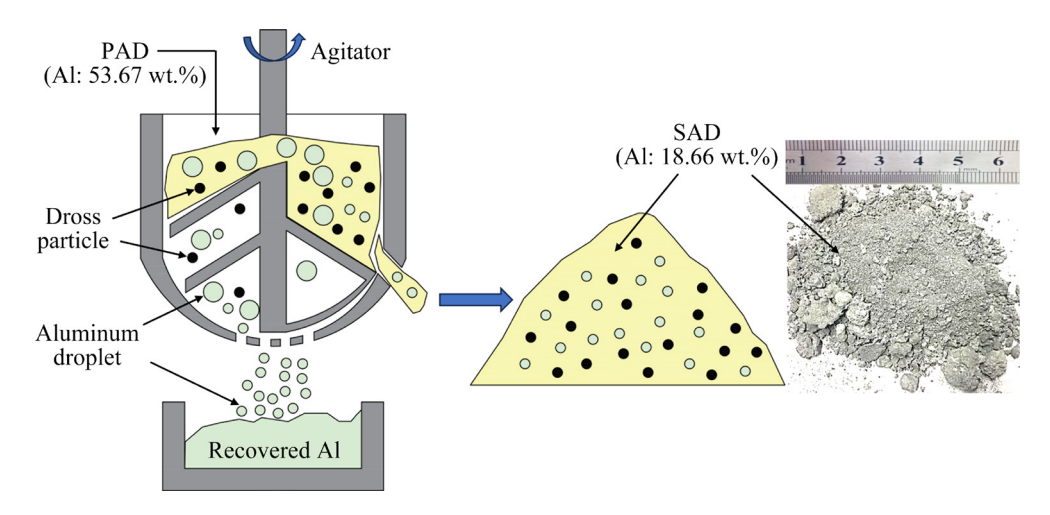


Fig. 1 Schematic diagram of aluminum extraction from PAD by agitation and formation of SAD

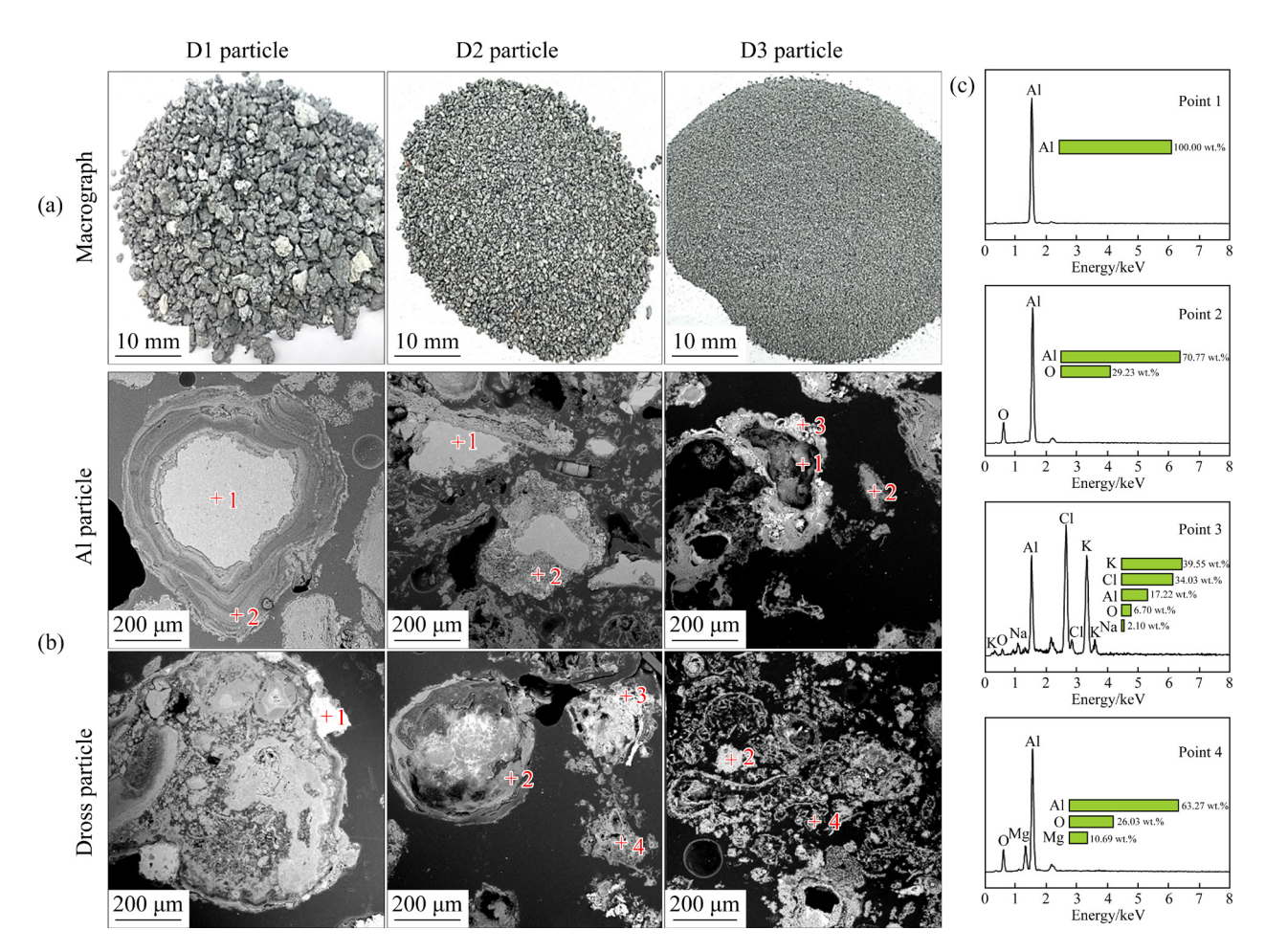


Fig. 2 Characterization of D1-D3 particles: (a) Macrographs; (b) SEM images; (c) EDS data

particular, the Al content of D1 and D2 particles was determined through a salt flux composed of 72 wt.% NaCl, 26 wt.% KCl, and 2 wt.% CaF<sub>2</sub>, following the method reported by DAVID and KOPAC [17]. In this method, a certain amount of the samples were melted in a graphite crucible at

750 °C, then cooled and washed. The exposed metallic aluminum particles were subsequently picked out. The mass ratio between the obtained metallic aluminum particles and the added samples was identified as the Al content of D1 and D2. The above method was not suitable for D3 particles due

to their small size and uniform distribution, so the mass fraction of Al in D3 particles was determined by the ICP-AES method.

The chemical compositions of D1, D2, and D3 particles are listed in Table 2, with Al contents of 27.68 wt.%, 14.82 wt.%, and 1.48 wt.%, respectively. The Al content of the raw material is calculated to be 18.66 wt.% based on mass balance calculations. The primary crystalline phases of D1-D3 particles in SAD include Al, MgAl<sub>2</sub>O<sub>4</sub>, Al<sub>2</sub>O<sub>3</sub>, AlN, and KCl, as presented by the XRD analysis results in Fig. 3. The microstructure and EDS data of metallic aluminum particles and dross particles in SAD with different particle sizes (D1-D3) are shown in Figs. 2(b, c). It is revealed that the metallic aluminum particles, with oxidized films attached to their surfaces, exist in various shapes and sizes. The dross particles are found to be mainly composed of non-metallic constituents with some fine metallic aluminum droplets entrained. The larger dross particles are nearly spherical with a

dense structure, while the finer dross particles seem to be integrated well with each other in an irregular form and show a loose and porous structure.

### 2.3 Experimental procedures

# 2.3.1 Characterization of surface structure of SAD particles treated by ball-milling

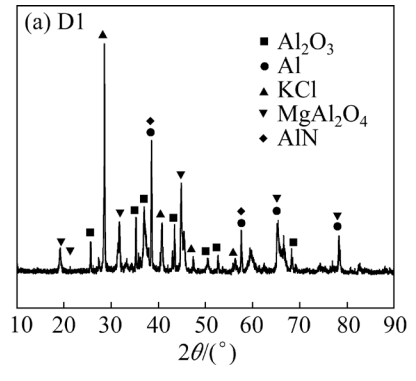
In general, the aluminum particles in SAD are covered with dense oxidized films, which makes it difficult to efficiently complete the separation and recovery of aluminum from SAD. Thus, original D1 and D2 particles were dry-milled employing a bench-scale ball mill equipped with a grinding medium of steel balls. The D3 particles were not treated and could be considered directly employed in the resource utilization due to fine particle size and low content of aluminum. The milling process was applied without water to avoid the effects of the reaction between AlN and H<sub>2</sub>O on the surface structure of aluminum particles, in which a certain amount of original D1 and D2 particles were added

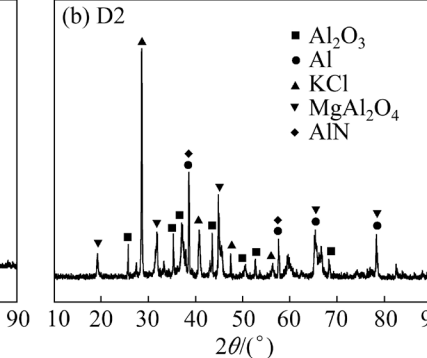
Table 1 Size distribution of SAD

Sample	Size/mm -	San	Retained			
		Upper	Middle	Bottom	Average	proportion/%
D1	>1.00	722.3	636.4	508.8	622.5	45.54
D2	0.300 - 1.00	491.9	517.8	605.6	538.4	39.39
D3	< 0.300	148.8	204.4	264.7	206.0	15.07
Total	-	1363.0	1358.6	1379.1	1366.9	100.00

Table 2 Chemical compositions of SAD (wt.%)

	Sample	Al	Al <sub>2</sub> O <sub>3</sub>	SiO <sub>2</sub>	MgO	K	Na	Cl	F	Others
	D1	27.68	37.48	7.22	12.34	3.12	3.26	4.49	0.98	3.43
	D2	14.82	43.26	6.98	15.75	4.25	2.06	6.75	1.28	4.85
	D3	1.48	48.42	8.49	18.29	5.41	1.83	8.08	2.32	5.68
_	Average	18.66	41.41	7.32	14.58	3.91	2.57	5.92	1.30	4.33





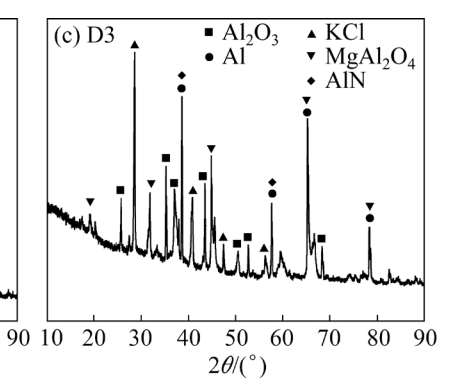


Fig. 3 XRD patterns for D1-D3 particles of SAD

to the ball mill and treated for 10 min. The SEM-EDS method was adopted to scanning the microstructure of aluminum particles in D1 and D2 before and after ball milling to evaluate the effect of milling on the surface structure of metallic aluminum particles.

## 2.3.2 In-situ observation on surface structure evolution of SAD particles with temperature

The effect of temperature and time on surface structure transformation of aluminum particles in D1 and D2 was examined in a Confocal Laser Scanning Microscope (CLSM) device equipped with an infrared furnace (VL2000DX; Lasertec Corporation) via in-situ observation. Three temperature points were adopted based on the melting point of aluminum (660 °C) and the refining temperature range of liquid aluminum. Each 1.0 g of milled D1 and D2 particles was heated to 680 °C, 710 °C, and 740 °C with a heating rate of 50 °C/min and held for different time. The transformation of the microstructure of aluminum particles in D1 and D2 was captured and recorded.

## 2.3.3 Supergravity-enhanced separation of metallic aluminum liquid from SAD

According to the variation of the surface structure of SAD at various temperatures with time, the separation of metallic aluminum liquid from SAD by supergravity was conducted in a laboratory installation illustrated in Fig. 4. The supergravity field generated from a centrifugal device, which primarily consists of a furnace with heating function and a counterweight, spins from vertical to horizontal as soon as it is turned on. The temperature of the experiment is jointly controlled via a conductive slip ring and a thermocouple attached to the sample, which allows real-time control of the temperature of the spinning sample within the stated accuracy range of ±3 °C. The rotation rate is varied by adjustment of the rotation rate controller united with a variable speed motor, and then the corresponding gravity coefficient can be calculated via Eq. (1). A nested graphite filter crucible, which was embedded with a layer of carbon fiber felt as the filter medium, was employed for the separation process.

$$G = \frac{\sqrt{g^2 + (\omega^2 x)^2}}{g} = \frac{\sqrt{g^2 + (\frac{N^2 \pi^2 x}{900})^2}}{g}$$
(1)

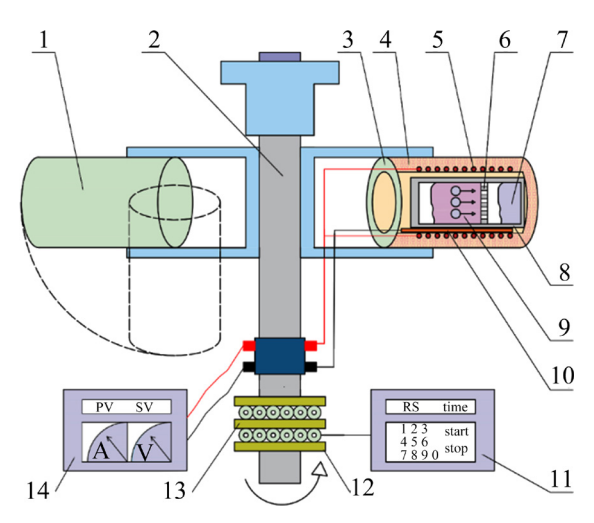


Fig. 4 Schematic diagram of experimental installation: 1 — Counterweight; 2 — Axis; 3 — Heating furnace; 4—Heat insulation layer; 5—Resistance wire; 6—Filter medium; 7—Aluminum liquid; 8—Graphite crucible; 9 — SAD; 10 — Thermocouple; 11 — Rotation rate controller; 12 — Conductive slip ring: fixing ring; 13 — Conductive slip ring: rotating ring; 14 — Temperature controller

where G is the gravity coefficient,  $\omega$  is the angular velocity (rad/s), g is the normal gravitational acceleration (g=9.80 m/s<sup>2</sup>), N is the rotating speed (r/min), and x is the distance from the centrifugal axis to the sample center (x=0.3 m).

Each 10 g of milled D1 and D2 particles was placed into the experimental crucibles. The heating furnace of the centrifugal device was heated to 680 °C and then the crucibles were put into the constant temperature zone of the heating furnace for 10 min, according to the transformation behavior of aluminum particles with temperature. Afterward, the centrifugal was launched and set to rotation speed of 546, 1092, and 1444 r/min to attain the gravity coefficients of *G*=100, 400, and 700 calculated via Eq. (1). The centrifugal was operated for 3 min, and then the crucible was removed quickly and air-cooled. Simultaneously, a contrast experiment was proceeded under the same conditions at normal gravity.

After the in-situ separation of aluminum liquid from the SAD particles by supergravity for 3 min, the mass of the products was weighed at first and the experimental samples were sectioned along the axial direction, and then the microstructure of the products on the filter was evaluated by the

SEM-EDS. The mass fraction of Al in the aluminum liquid was measured by the ICP-AES method, and the Al recovery ratio in the aluminum liquid separated from D1, D2, and SAD was calculated via Eq. (2) and Eq. (3):

$$R_{\text{Al}i} = \frac{m_{\text{Al}i\text{-separated}} \cdot w_{\text{Al}i\text{-separated}}}{m_{\text{Al}i} \cdot w_{\text{Al}i}} \times 100\%$$
 (2)

$$R_{\text{TAI}} = \frac{\sum m_{\text{Al}i} \cdot w_{\text{Al}i} \cdot R_{\text{Al}i}}{\sum m_{\text{Al}i} \cdot w_{\text{Al}i}} \times 100\%$$
 (3)

where  $R_{Ali}$  is the Al recovery ratio in aluminum liquid separated from D1 and D2 particles (i=1, 2),  $R_{TAl}$  is the total Al recovery ratio in the aluminum liquid separated from SAD,  $m_{Ali\text{-separated}}$  and  $w_{Ali\text{-separated}}$  are the mass and Al content of the separated aluminum liquid from D1 and D2 particles (i=1, 2),  $m_{Ali}$  and  $w_{Ali}$  are the mass and Al content of the added aluminum particles (i=1, 2, 3).

### 3 Results and discussion

### 3.1 Effect of ball-milling on surface structure of SAD particles

Figure 5 compares the variations in the surface and cross-sectional structures of metallic aluminum particles in D1 and D2 before and after ball-milling. The microscopic existence states of the original D1 and D2 particles are exhibited in Figs. 5(a, b), respectively. The structure of metallic aluminum particles can be categorized into four forms, including no obvious oxidized films, an oxidized layer covering the entire surface, a nonconsecutive oxidized layer attached to the surface, and a compact and complex network structure composed of MgAl<sub>2</sub>O<sub>4</sub> and Al<sub>2</sub>O<sub>3</sub> attached to the surface.

Figures 5(c, d) testify that the oxidized layer

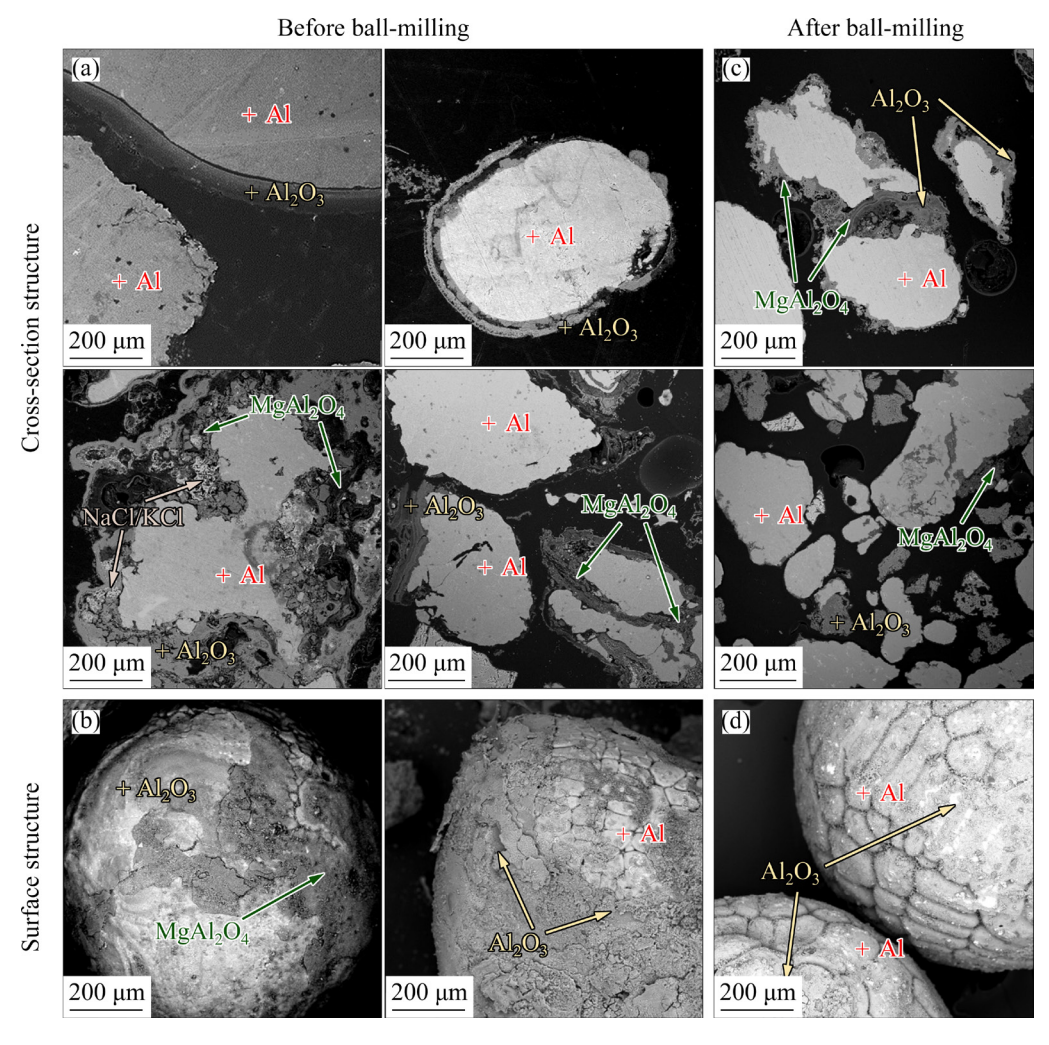


Fig. 5 Variations in microstructures of metallic aluminum particles in D1 and D2: (a, b) Before ball-milling; (c, d) After ball-milling

structure of regular-shaped metallic aluminum particles was broken and became thinner after ball-milling. In the meantime, the compact and complex network structure attached to the surfaces of irregular-shaped metallic aluminum particles was mostly stripped away [33]. As a result, the aluminum surface was extensively exposed. These changes in the surface structure of metallic aluminum particles can be significantly attributed to the mechanical actions of ball-milling, such as impact, grinding, and shearing.

### 3.2 In-situ observation on surface structure evolution of SAD particles with temperature

Figure 6 further illustrates the in-situ observation of the surface structure of milled D1 and D2 particles with varying temperature and time.

The results indicate that the milled D1 and D2 particles began to melt at 680 °C within 10 min, with the surface structure remaining almost intact initially. They were then completely melted to a liquid state with the time increasing to 20-30 min. As the temperature rose to 710–740 °C, the shape of the molten aluminum drops in the milled D1 and D2 particles began to change and became more irregular, and some of them were oxidized again. Additionally, due to high interfacial tension and poor fluidity, the aluminum liquid in D1 and D2 could not separate from the oxides and flow freely under normal gravity conditions within 30 min [34]. Based on these observations, the solid-liquid separation was conducted at 680 °C using supergravity to release and recover metallic aluminum droplets from SAD.

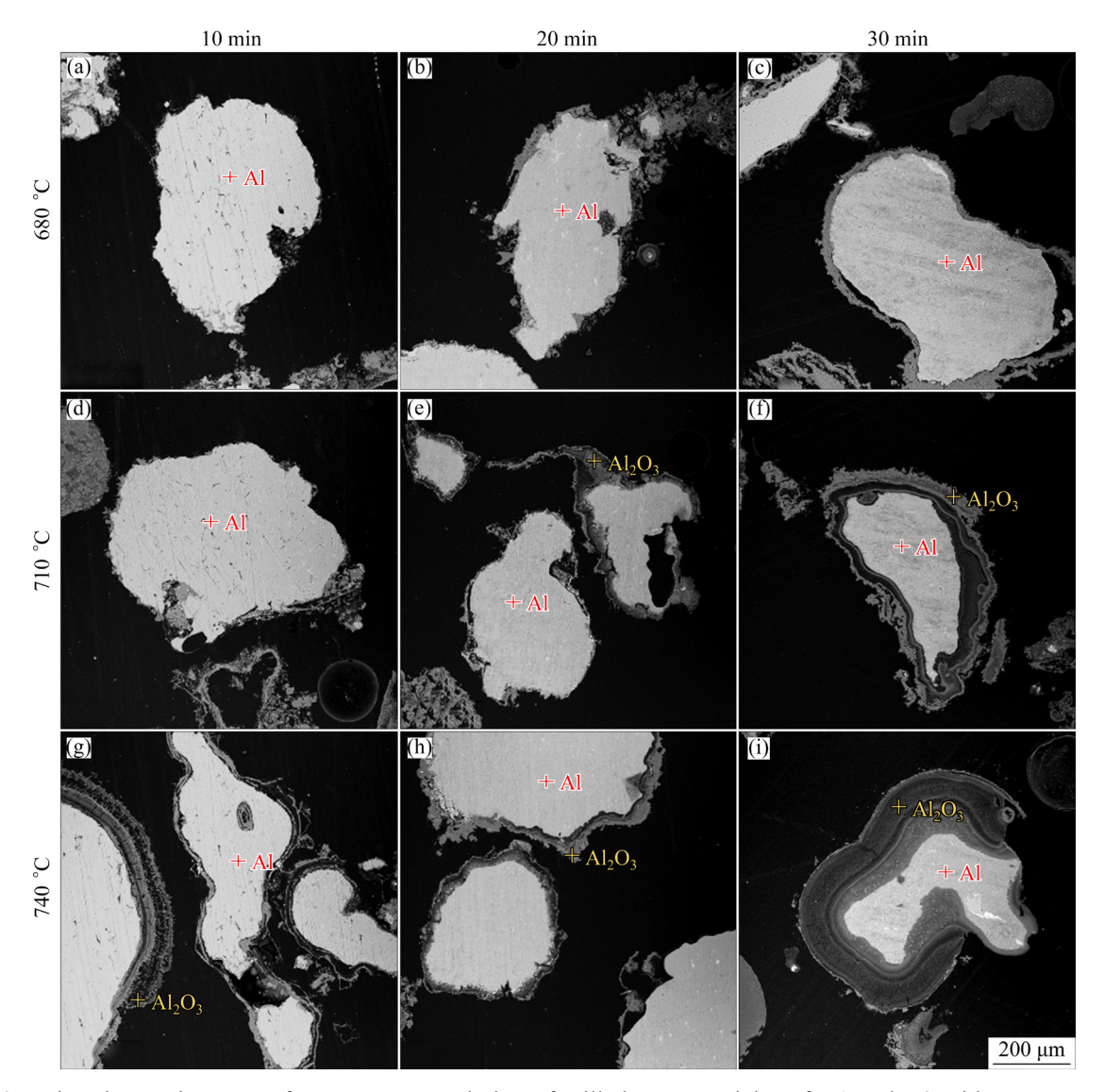


Fig. 6 In-situ observation on surface structure evolution of milled SAD particles of D1 and D2 with temperature and time

### 3.3 Supergravity-enhanced separation of metallic aluminum liquid from SAD

Based on the observed in-situ evolution of the surface structure of milled SAD particles with temperature, the separation of metallic aluminum liquid from the SAD was conducted at 680 °C via supergravity-enhanced separation. The macroscopic morphologies of SAD with particle sizes of D1 and D2 obtained under various gravity coefficients are

shown in Fig. 7. As demonstrated in Figs. 7(a, c), even if the oxidized films of aluminum particles had been greatly broken through ball-milling, the metallic aluminum liquid remained difficult to release from the oxidized films due to the strong mechanical stability between the aluminum liquid and solid films. Consequently, almost no metallic aluminum liquid was separated from the SAD under normal gravity (G=1).

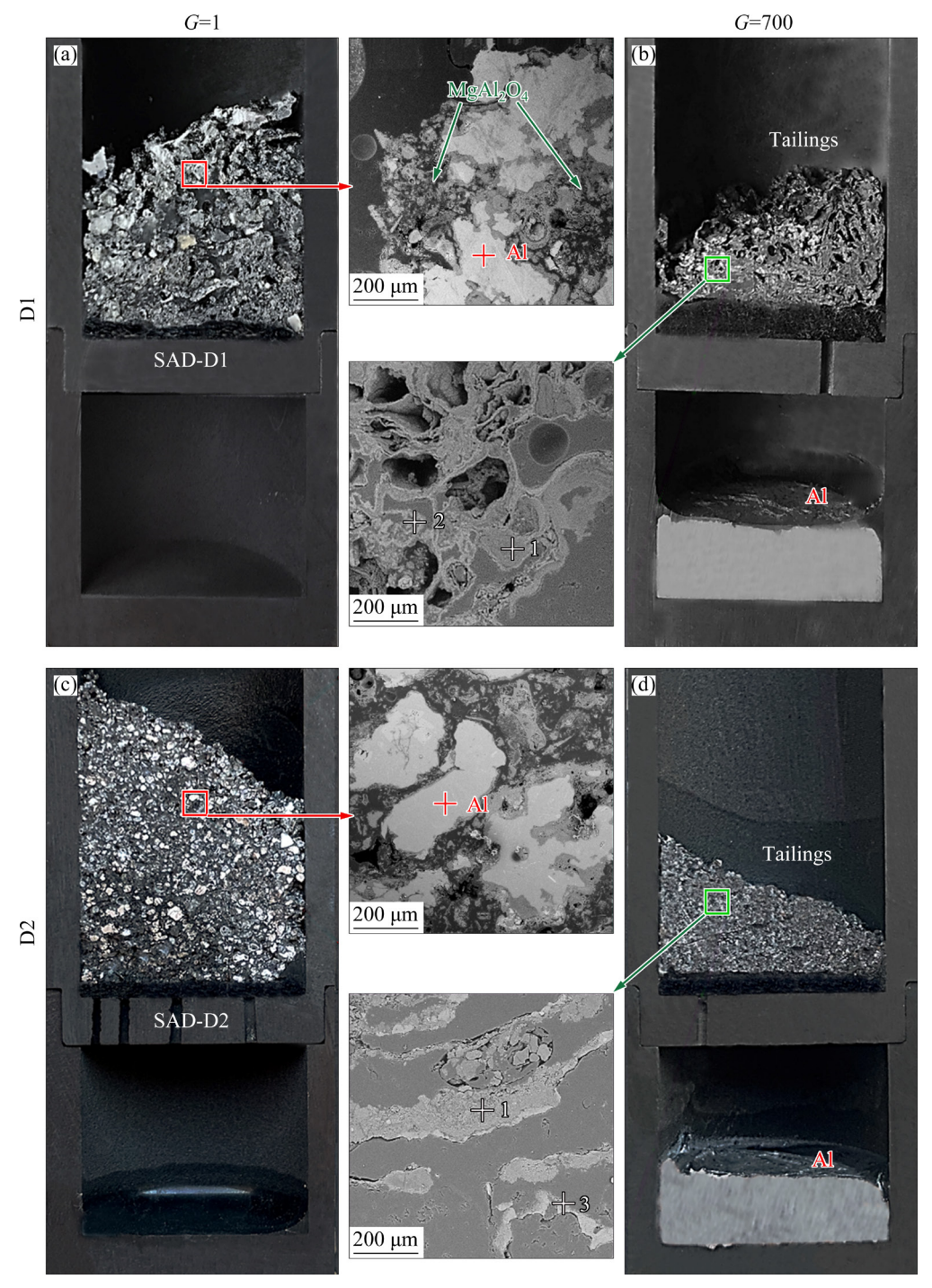


Fig. 7 Macroscopic morphology of SAD with particle sizes of D1 and D2 attained via supergravity-enhanced separation at 680 °C for 3 min

The driving force for solid–liquid separation was considerably improved under supergravity, resulting in significant release and separation of aluminum from the SAD with both sizes of D1 and D2, as displayed in Figs. 7(b–d) and Table 3. Figures 7(b–d) further exhibit the microstructure of the tailings intercepted by the filter, which indicated that the separation of metallic aluminum droplets from D1 and D2 was significantly enhanced with the increase of gravity coefficient, and only the oxidized films mainly composed of  $Al_2O_3$  and  $MgAl_2O_4$  remained in the tailings under the condition of G=700.

**Table 3** EDS data of phases in tailings obtained from supergravity-enhanced separation of SAD

1 6				1					
Point		Content/wt.%							
in Fig. 7	Al	Mg	Si	K	O	N	Cl	Phase	
1	61.46	9.35			29.19			$\begin{array}{c} Al_2O_3/\\ MgAl_2O_4 \end{array}$	
2	41.62		2.81	6.66	40.70		8.21	KCl/ Al <sub>2</sub> O <sub>3</sub>	
3	60.55	2.40			19.08	17.97		AlN/ Al <sub>2</sub> O <sub>3</sub>	

The SEM-EDS image and XRD peaks of aluminum separated from SAD enhanced by supergravity are depicted in Fig. 8, indicating a higher purity of the recovered aluminum. The variations in mass fractions and recovery ratio of Al in the separated aluminum liquid from SAD with gravity coefficient are shown further in Fig. 9. It was testified that aluminum was greatly recovered from the SAD with both sizes of D1 and D2 as the gravity coefficient elevated to 700 from 100, and the R<sub>TAI</sub> was up to 95.72% as calculated based on Eq. (3). The mass fractions of Al in the separated aluminum from the SAD with the sizes of D1 and D2 were up to 99.18% and 99.10%. In contrast, the mass fractions of Al in the tailings from the SAD with sizes of D1 and D2 were decreased to 0.66% and 0.84%. Hence, considering the low Al content in these two products, the SAD with the size of D3 and the tailings can be easily utilized further in related fields.

#### 3.4 Discussion

### 3.4.1 Process for aluminum recovery from SAD

It is well-known that SAD, rooted during the aluminum extraction from PAD, constitutes a

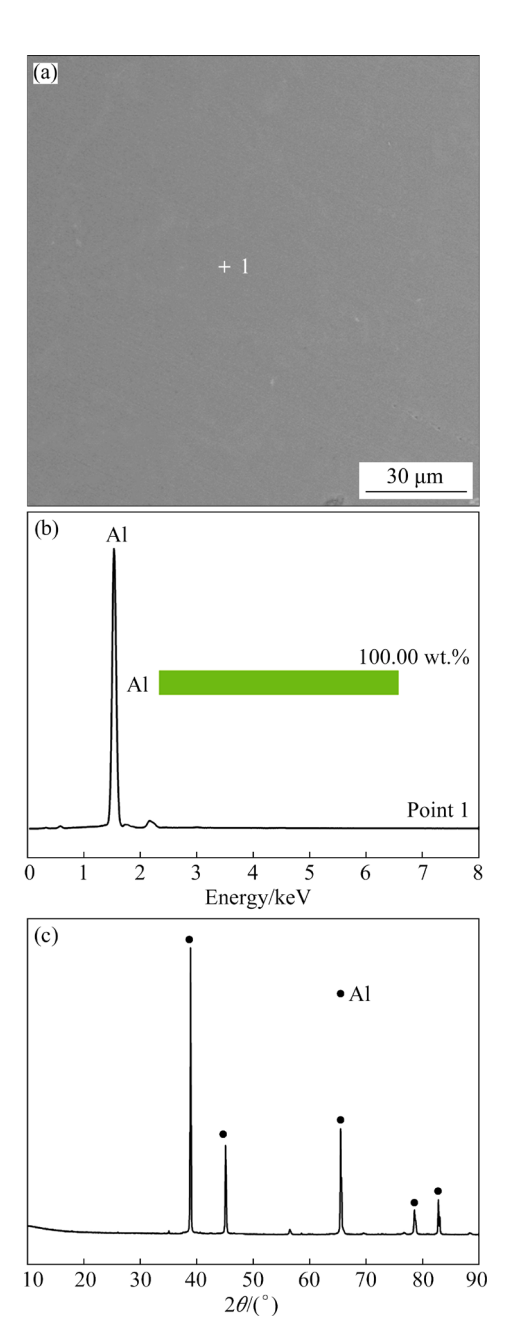


**Fig. 8** SEM-EDS image and XRD pattern of metallic aluminum recovered from SAD via supergravity-enhanced separation: (a) SEM image; (b) EDS data of metallic aluminum; (c) XRD pattern

hazardous solid waste due to its leachability and reactivity. Despite containing significant amounts of metallic aluminum particles, SAD remains challenging to recover using conventional methods due to its heavy coating of oxidized films. In this study, a novel method was proposed for the efficient recovery of metallic aluminum and the sustainable utilization of SAD via ball-milling and supergravity-enhanced separation, and the flow chart for this process is shown in Fig. 10.

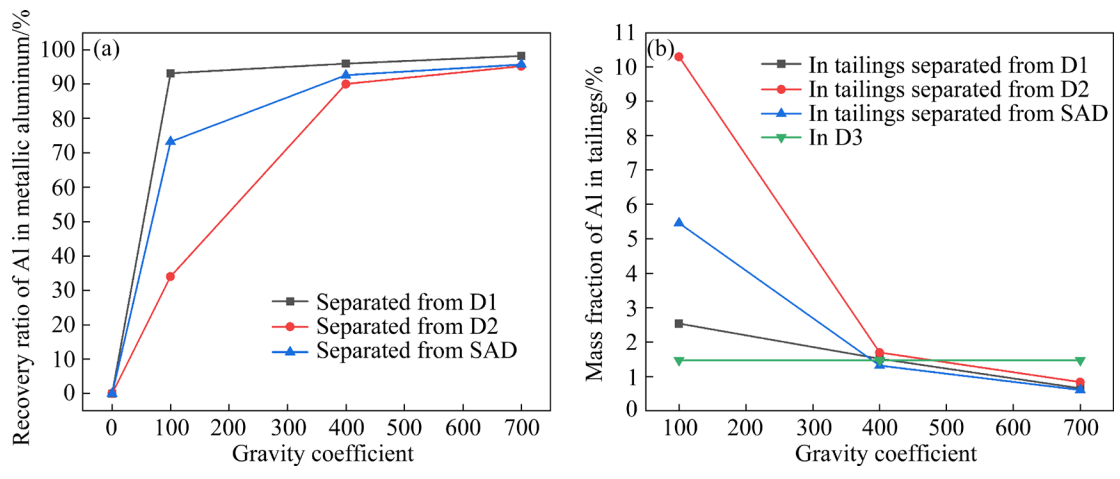


Fig. 9 Recovery and mass fraction of Al in metallic aluminum and tailings separated from SAD enhanced by supergravity field: (a) Recovery ratio; (b) Mass fraction

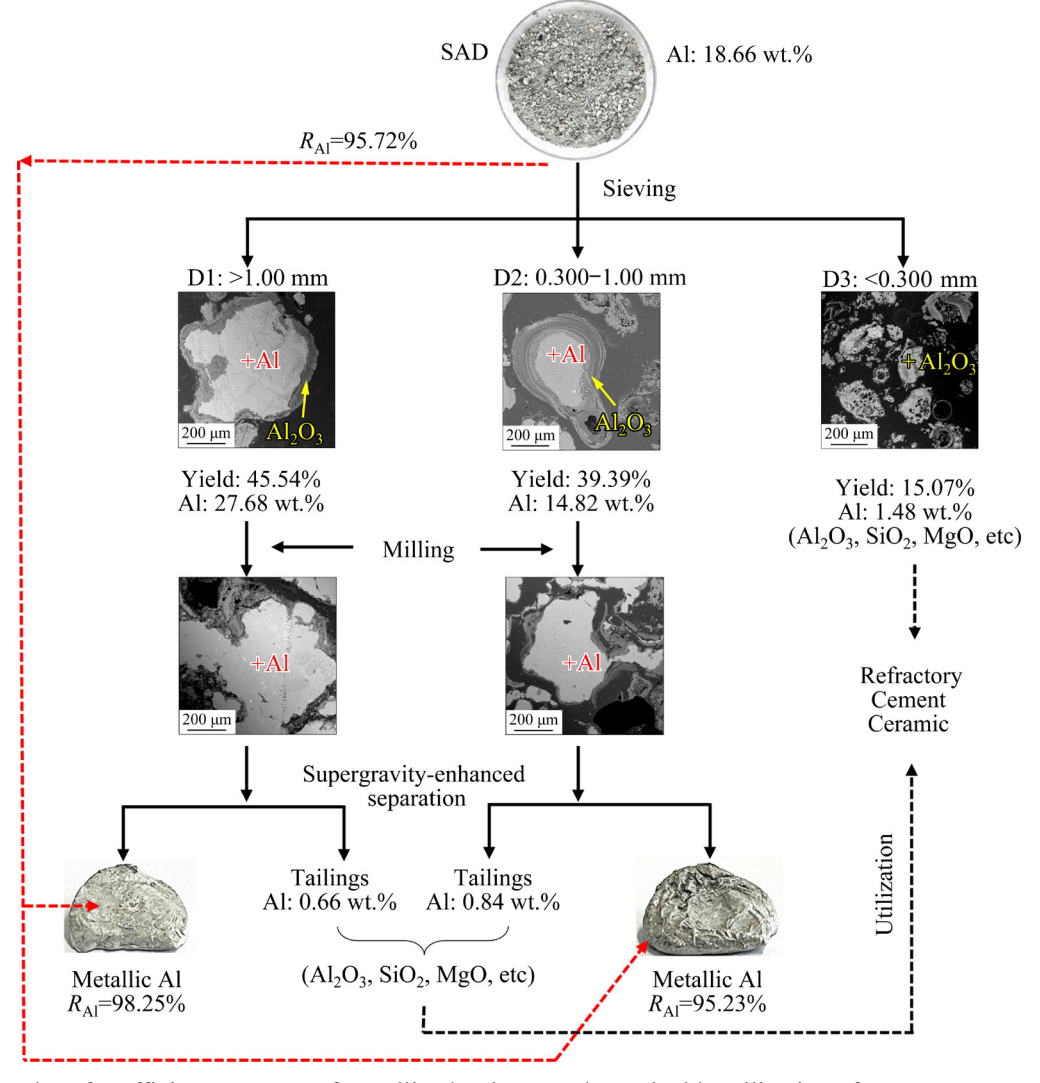


Fig. 10 Flow chart for efficient recovery of metallic aluminum and sustainable utilization of SAD

Initially, the solid films of aluminum particles are significantly disrupted through ball-milling, creating conditions conducive to releasing metallic

aluminum droplets from the oxidized films of SAD. However, due to the substantial interfacial tension between the metallic aluminum droplets and oxidized films, it proves challenging to drive the aluminum liquid to move and separate from the SAD under normal gravity conditions (G=1). Consequently, the supergravity field is employed to enhance driving force and facilitate solid—liquid separation, resulting in the release and recovery of aluminum from the solid films in the SAD with a high recovery ratio.

Combining our previous study [35], the method introduced in this study efficiently recovers aluminum not only from larger PAD but also from smaller SAD particles. Nowadays, the ball-milling process is very mature in the industry. Supergravityenhanced separation technology offers significant potential advantages in mass transfer and phase migration, making it a promising option for industrial application. However, before widespread adoption, it is essential to develop novel facilities suitable for industrial-scale production and optimize the coordination among various processes. In general, decanter centrifuges are more suitable for solid-liquid separation of aluminum from SAD in industrial settings [36]. Therefore, we have developed and manufactured a centrifugal device for horizontal installation. Currently, we are addressing some limitations of this equipment, such as the design of the filter and the feed of SAD, and we are committed to continually improving our facility and conducting tests for industrial applications at the earliest opportunity.

To estimate the economic feasibility of this technology, a cost analysis was conducted based on the current market price of raw materials, actual experimental data, and corrected energy consumption. The energy consumption was in the form of electricity and was transformed into the mass of standard coal. The calculation results are listed in Table 4, indicating that this technology

has great economic benefits, approximately RMB  $\Upsilon$  309.52–338.19 can be gained for each treatment of 100 kg SAD.

3.4.2 Harmless and resource utilization of tailings

Due to the adequate migration of aluminum liquid from SAD, the remaining tailings are composed of 78.26% Al<sub>2</sub>O<sub>3</sub>, 7.34% MgO, 4.76% SiO<sub>2</sub>, and small amounts of AlN, chlorides, and fluorides. These tailings can be sustainably utilized further in the fields of refractory [37], cement [18], and ceramic [19], owing to the high-temperature resistance and chemical stability of Al<sub>2</sub>O<sub>3</sub> and MgO. However, before such utilization, it is necessary to treat the tailings harmlessly.

The tailings containing AlN and salt can be treated further using hydrometallurgy or pyrometallurgy methods. Initially, the hydrolysis of AlN and the dissolution of salt readily occur when the tailings are immersed in water [38]. The ammonia generated from AlN hydrolysis is typically collected by a gas treatment system, while the dissolved salt can be recovered through evaporation and concentration. Consequently, the final treated tailings can be safely utilized for refractory preparation without any risk.

Furthermore, ZHU et al [34] conducted a review on the denitrification, dechlorination, and fluoride fixation of SAD and performed a feasibility analysis of the synergistic conversion of multipollutant using the pyrometallurgical process. The findings indicate that the chlorides can be evaporated at a specific temperature [39]. Additionally, AlN transforms into stable  $\alpha$ -Al<sub>2</sub>O<sub>3</sub> from amorphous Al<sub>2</sub>O<sub>3</sub> during oxidation at higher temperatures ranging from 600 to 1300 °C [40,41].

Given that AlN is reductive, SHEN et al [42,43] employed SAD to reduce and recover heavy metals in pickled sludge and performed glass ceramics

Table 4 Economic estimation and feasibility of proposed technology

Item	Energy/kJ	Mass/kg	Cost/RMB¥
SAD	_	100.00	_
Materials preparation	142850-186750	4.87-6.37	12.39-16.21
Ball-milling	73900-88400	2.52-3.02	6.41-7.68
Supergravity separation	53850-68400	1.84-2.33	4.68-5.93
Tailings	_	82.14	_
Aluminum	_	17.86	339.34-361.67
_	_	_	309.52-338.19
	SAD  Materials preparation Ball-milling Supergravity separation Tailings	SAD –  Materials preparation 142850–186750  Ball-milling 73900–88400  Supergravity separation 53850–68400  Tailings –	SAD         -         100.00           Materials preparation         142850-186750         4.87-6.37           Ball-milling         73900-88400         2.52-3.02           Supergravity separation         53850-68400         1.84-2.33           Tailings         -         82.14

fabrication. Fluorides in SAD are dissociated at reduction temperature and fixed in the form of CaF<sub>2</sub> because pickled sludge contains a considerable amount of CaO, which further reduces the viscosity of slag and promotes the recovery of chromium and nickel [9,42]. Furthermore, XIE et al [44] proposed an approach for the joint disposal of various industrial hazardous wastes to facilitate collaborative detoxification and extraction of valuable resources, including aluminum dross, carbide slag, coal gangue, red mud, and spent cathode carbon blocks.

Hence, the study presented in this work combined with the research mentioned above, provides ideas and foundations for the efficient extraction of metallic aluminum from SAD and the subsequent disposal and utilization of tailings.

#### 4 Conclusions

- (1) The surface structure of SAD particles before and after ball-milling was studied, and it was found that the oxidized films of metallic aluminum particles with different sizes of >1.00 mm, and 0.300–1.00 mm were greatly broken.
- (2) Based on the in-situ observation of surface structure evolution of milled SAD particles with temperature, solid-liquid separation was conducted at 680 °C enhanced by a supergravity field to release and separate metallic aluminum liquid in SAD.
- (3) The metallic aluminum liquid was efficiently recovered from the SAD via supergravity-enhanced separation, where the recovery ratio and mass fraction of Al was up to 95.72% and 99.10% at G=700, and the tailings mainly consisting of Al<sub>2</sub>O<sub>3</sub>, SiO<sub>2</sub>, and MgO can be used in refractory, cement, and ceramic sustainably.

### **CRediT** authorship contribution statement

Zeng-wu WANG: Methodology, Formal analysis, Investigation, Writing – Original draft; Jing-tao GAO: Conceptualization, Writing – Review & editing; Xi LAN: Data curation, Visualization, Validation; Zhan-cheng GUO: Funding acquisition, Resources, Supervision.

### **Declaration of competing interest**

The authors declare that they have no known competing financial interests or personal relationships that could have appeared to influence the work reported in this paper.

#### Acknowledgments

This study was supported by the National Natural Science Foundation of China (Nos. 52304342, 52174275, 51774037) and the China Postdoctoral Science Foundation (No. 2021M700393)

#### References

- [1] ZHOU Guo-tao, WANG Yi-lin, QI Tian-gui, ZHOU Qiu-sheng, LIU Gui-hua, PENG Zhi-hong, LI Xiao-bin. Enhanced conversion mechanism of Al-goethite in gibbsitic bauxite under reductive Bayer digestion process [J]. Transactions of Nonferrous Metals Society of China, 2022, 32: 3077–3087.
- [2] CUI Ji-rang, J.ROVEN H. Recycling of automotive aluminum [J]. Transactions of Nonferrous Metals Society of China, 2010, 20: 2057–2063.
- [3] YANG Yi, GUO Yao-qi, ZHU Wen- song, HUANG Jian-bai. Environmental impact assessment of China's primary aluminum based on life cycle assessment [J]. Transactions of Nonferrous Metals Society of China, 2019, 29: 1784–1792.
- [4] SRIVASTAVA A, MESHRAM A. On trending technologies of aluminum dross recycling: A review [J]. Process Safety and Environmental Protection, 2023, 171: 38–54.
- [5] MAROPOULOS S, KOUNTOURAS D, VOULGARAKI X, PAPANIKOLAOU S, SANAIDIS I. A characterization method for Al recovery from dross based on compression at elevated temperatures [J]. Advances in Tribology, 2011, 2011: 395716.
- [6] SHINZATO M C, HYPOLITO R. Solid waste from aluminum recycling process: characterization and reuse of its economically valuable constituents [J]. Waste Management, 2005, 25(1): 37–46.
- [7] HIRAKI T, NAGASAKA T. An easier upgrading process of aluminum dross residue by screening technique [J]. Journal of Material Cycles and Waste Management, 2015, 17(3): 566-573.
- [8] DAS B R, DASH B, TRIPATHY B C, BHATTACHARYA I N, DAS S C. Production of g-alumina from waste aluminum dross [J]. Minerals Engineering, 2007, 20(3): 252–258.
- [9] GAO Qin, GUO Qiang, LI Yong-li, REN Bao-zeng, FU Ming-bo, LI Hui-lin, TIAN Deng-chao, DING Min. Innovative technology for defluorination of secondary aluminum dross by alkali leaching [J]. Minerals Engineering, 2021, 172: 107134.
- [10] Environmental Protection Agency. European waste catalogue and hazardous waste list [R]. Ireland, 2002–01–01.
- [11] LI Wen-hao, ZHANG Xiao-yan, ZHANG Jun-jie, SHEN Han-lin, YANG Jun-jie, LIU Ying, LIU Jun, ZHANG Shen-gen, YANG Jin-long. Porous ceramics with near-zero shrinkage and low thermal conductivity from hazardous secondary aluminum dross [J]. Journal of the American Ceramic Society, 2022, 105(5): 3197–3210.
- [12] MESHRAM A, SINGH K K. Recovery of valuable products from hazardous aluminum dross: A review [J]. Resources, Conservation and Recycling, 2018, 130: 95–108.

- [13] LI Yong, QIN Zi-yi, LI Chun-lei, QU Yi, WANG Hai-bin, PENG Li, WANG Yi. Hazardous characteristics and transformation mechanism in hydrometallurgical disposing strategy of secondary aluminum dross [J]. Journal of Environmental Chemical Engineering, 2021, 9(6): 106470.
- [14] MAHINROOSTA M, ALLAHVERDI A. Hazardous aluminum dross characterization and recycling strategies: A critical review [J]. Journal of Environmental Management, 2018, 223: 452–468.
- [15] HU K T, REED D, ROBSHAW T J, SMITH R M, OGDEN M D. Characterisation of aluminium black dross before and after stepwise salt-phase dissolution in non-aqueous solvents [J]. Journal of Hazardous Materials, 2021, 401: 123351.
- [16] ZHU Xue-yuan, JIN Qiang, YE Zhen. Life cycle environmental and economic assessment of alumina recovery from secondary aluminum dross in China [J]. Journal of Cleaner Production, 2020, 277: 123291.
- [17] DAVID E, KOPAC J. Aluminum recovery as a product with high added value using aluminum hazardous waste [J]. Journal of Hazardous Materials, 2013, 261: 316–324.
- [18] ZHANG Shi-yu, REN Feng-yu, DING Hang-xing, QIU Jing-ping, TIAN Yan-sheng, LIU Na. Recycling aluminum dross as a mineral admixture in CaO-activated superfine slag [J]. Construction and Building Materials, 2021, 279: 122434.
- [19] ZHU Wei-jun, WU Kang-kai, ZHANG Sen-jing, LIU Jun, YI Xue-mei, ZHANG Li-hua. Zero-Waste progress for the synthesis of high-purity β-sialon ceramics from secondary aluminum dross [J]. Advanced Engineering Materials, 2021, 23(4): 2001298.
- [20] ADEOSUN S O, AKPAN E I, DADA M O. Refractory characteristics of aluminum dross-kaolin composite [J]. JOM, 2014, 66(11): 2253–2261.
- [21] HONG Jian-ping, WANG Jun, CHEN Hai-yan, SUN Bao-de, LI Jia-jing, CHEN Chong. Process of aluminum dross recycling and life cycle assessment for Al–Si alloys and brown fused alumina [J]. Transactions of Nonferrous Metals Society of China, 2010, 20: 2155–2161.
- [22] SARKER M S R, ALAM M Z, QADIR M R, GAFUR M A. Moniruzzaman, extraction and characterization of alumina nanopowders from aluminum dross by acid dissolution process [J]. International Journal of Minerals, Metallurgy, and Materials, 2015, 22(4): 429–436.
- [23] JIMÉNEZ A, RIVES V, VICENTE M A, GIL A. A comparative study of acid and alkaline aluminum extraction valorization procedure for aluminum saline slags [J]. Journal of Environmental Chemical Engineering, 2022, 10: 107546.
- [24] HE Liu-qing, SHI Lin, HUANG Qi-zhen, HAYAT Waseem, SHANG Zhong-bo, MA Teng-fei, WANG Min, YAO Wei-dong, HUANG Hao-yong, CHEN Rui. Extraction of alumina from aluminum dross by a non-hazardous alkaline sintering process: Dissolution kinetics of alumina and silica from calcined materials [J]. Science of the Total Environment, 2021, 777: 146123.
- [25] TURK M, ALTINER M, TOP S, KARACA S, BOUCHEKRIT C. Production of alpha-alumina from black aluminum dross using NaOH leaching followed by calcination [J]. JOM, 2020, 72(10): 3358–3366.
- [26] SARAVANAKUMAR R, RAMACHANDRAN K, LALY L G, ANANTHAPADMANABHAN P V, YUGESWARAN S.

- Plasma assisted synthesis of γ-alumina from waste aluminium dross [J]. Waste Management, 2018, 77: 565–575
- [27] MAHINROOSTA M, ALLAHVERDI A, DONG P, BASSIM N. Green template-free synthesis and characterization of mesoporous alumina as a high value-added product in aluminum black dross recycling strategy [J]. Journal of Alloys and Compounds, 2019, 792: 161–169.
- [28] FENG Hai-gang, ZHANG Guo-fan, YANG Qun, XUN Luo-bing, ZHEN Si-yuan, LIU De-zhi. The investigation of optimizing leaching efficiency of Al in secondary aluminum dross via pretreatment operations [J]. Processes, 2020, 8(10): 1269.
- [29] YOLDI M, FUENTES-ORDOÑEZ E G, KORILI S A, GIL A. Zeolite synthesis from aluminum saline slag waste [J]. Powder Technology, 2020, 366: 175–184.
- [30] NGUYEN T T N, SONG S J, LEE M S. Development of a hydrometallurgical process for the recovery of pure alumina from black dross and synthesis of magnesium spinel [J]. Journal of Materials Research and Technology, 2020, 9(2): 2568–2577.
- [31] LAN Xi, GAO Jin-tao, LI Yu, GUO Zhan-cheng. A green method of respectively recovering rare earths (Ce, La, Pr, Nd) from rare-earth tailings under super-gravity [J]. Journal of Hazardous Materials, 2019, 367: 473–481.
- [32] LAN Xi, GAO Jin-tao, QU Xin-tuo, GUO Zhan-cheng. An environmental-friendly method for recovery of soluble sodium and harmless utilization of red mud: Solidification, separation, and mechanism [J]. Resources, Conservation and Recycling, 2022, 186: 106543.
- [33] DAVID E, KOPAC J. Hydrolysis of aluminum dross material to achieve zero hazardous waste [J]. Journal of Hazardous Materials, 2012, 209: 501–509.
- [34] ZHU Xing-han, YANG Jin-zhong, YANG Yu-fei, HUANG Qi-fei, LIU Tao. Pyrometallurgical process and multipollutant co-conversion for secondary aluminum dross: A review [J]. Journal of Materials Research and Technology, 2022, 21: 1196–1211.
- [35] WANG Zeng-wu, GAO Jin-tao, LAN Xi, FENG Guo-liang, GUO Zhan-cheng. An environmental-friendly method for recovery of aluminum droplets from aluminum dross: Mechanical activation and super-gravity separation [J]. Process Safety and Environmental Protection, 2023, 175: 199–211.
- [36] ANLAUF H. Recent developments in centrifuge technology [J]. Separation and Purification Technology, 2007, 58: 242–246.
- [37] SHEN Han-lin, LIU Bo, ZHAO Shi-zhen, ZHANG Jun-jie, YUAN Jing-shu, ZHANG Yao, ZHANG Shen-gen. Iron oxide and jadeite nucleation in high alumina glass-ceramics prepared from secondary aluminum dross [J]. Ceramics International, 2021, 47(15): 21744–21750.
- [38] ZHANG Yong, GUO Zhao-hui, HAN Zi-yu, XIAO Xi-yuan. Effects of AlN hydrolysis on fractal geometry characteristics of residue from secondary aluminium dross using response surface methodology [J]. Transactions of Nonferrous Metals Society of China, 2018, 28: 2574–2581.
- [39] LI Jia-jing, WANG Jun, CHEN Hai-yan, SUN Bao-de. Influence of hot pressing sintering temperature on β-Sialon-15R ceramics synthesized from aluminum dross [J].

- Materials Transactions, 2012, 53: 1495-1501.
- [40] LIN Chih-yuan, LU Fu-hsing. Oxidation behavior of AlN films at high temperature under controlled atmosphere [J]. Journal of the European Ceramic Society, 2008, 28: 691–698.
- [41] XIE Hui-min, GUO Zhao-hui, XU Rui, ZhANG Yang-lin, XU Zhi. Synergistic effect of inorganic salt and AlN removal in the secondary aluminum dross during the roasting process [J]. Journal of Alloys and Compounds, 2022, 966: 171518.
- [42] SHEN Han-lin, LIU Bo, SHI Zhi-sheng, ZHAO Shi-zhen, ZHANG Jun-jie, ZHANG Shen-gen. Reduction for heavy metals in pickling sludge with aluminum nitride in secondary

- aluminum dross by pyrometallurgy, followed by glass ceramics manufacture [J]. Journal of Hazardous Materials, 2021, 418: 126331.
- [43] SHEN Han-lin, LIU Bo, ZHANG Jun-jie, LIU Jun, ZHANG Shen-gen. Homogeneous reduction for heavy metals from pickling sludge with aluminum nitride from secondary aluminum dross in aluminosilicate melt 'solution' environment [J]. Journal of Cleaner Production, 2022, 362: 132358.
- [44] XIE Ming-zhuang, LIU Feng-qin, SHI Li-tao, ZHAO Hong-liang. Green synthesis of aluminum hydroxide from alumina-silica based solid hazardous waste [J]. Environmental Technology & Innovation, 2023, 30: 103127.

### 球磨-超重力强化分离法高效回收二次铝渣中的金属铝

汪增武, 高金涛, 兰 茜, 郭占成

北京科技大学 绿色低碳钢铁冶金全国重点实验室, 北京 100083

摘 要:二次铝渣(SAD)是原铝渣提铝过程中产生的一种副产物,含有大量被致密氧化膜包裹着的金属铝颗粒,因此难以用传统方法高效回收金属铝。采用球磨破坏和改变氧化膜的结构。结果表明,球磨使氧化膜变薄并剥离,从而暴露出铝表面。根据对球磨后 SAD 颗粒结构随温度变化的原位观察结果,在 680 ℃下通过超重力强化分离法从 SAD 中高效回收金属铝液,分离出的铝相中铝的回收率和质量分数分别达 95.72%和 99.10%。此外,尾渣后续经脱氮、脱氯和固氟等无害化处理后,可在耐火材料、水泥和陶瓷等领域实现资源利用。

关键词:二次铝渣(SAD);金属铝;高效回收;球磨;超重力强化分离

(Edited by Bing YANG)